

Article

Conformer-Specific Dissociation Dynamics in Dimethyl Methylphosphonate Radical Cation

Vaibhav Singh ¹, Hugo A. López Peña ², Jacob M. Shusterman ², Patricia Vindel-Zandbergen ³, Katharine Moore Tibbetts ² and Spiridoula Matsika ^{1,*}¹ Department of Chemistry, Temple University, Philadelphia, PA 19122, USA; vaibhav.singh@temple.edu² Department of Chemistry, Virginia Commonwealth University, Richmond, VA 23284, USA; lopezpenaha@vcu.edu (H.A.L.P.); shustermaj@vcu.edu (J.M.S.); kmtibbetts@vcu.edu (K.M.T.)³ Department of Physics, Rutgers University at Newark, Newark, NJ 07102, USA; pv.zandbergen@rutgers.edu

* Correspondence: smatsika@temple.edu

Abstract: The dynamics of the dimethyl methylphosphonate (DMMP) radical cation after production by strong field adiabatic ionization have been investigated. Pump-probe experiments using strong field 1300 nm pulses to adiabatically ionize DMMP and a 800 nm non-ionizing probe induce coherent oscillations of the parent ion yield with a period of about 45 fs. The yields of two fragments, $\text{PO}_2\text{C}_2\text{H}_7^+$ and PO_2CH_4^+ , oscillate approximately out of phase with the parent ion, but with a slight phase shift relative to each other. We use electronic structure theory and nonadiabatic surface hopping dynamics to understand the underlying dynamics. The results show that while the cation oscillates on the ground state along the P=O bond stretch coordinate, the probe excites population to higher electronic states that can lead to fragments $\text{PO}_2\text{C}_2\text{H}_7^+$ and PO_2CH_4^+ . The computational results combined with the experimental observations indicate that the two conformers of DMMP that are populated under experimental conditions exhibit different dynamics after being excited to the higher electronic states of the cation leading to different dissociation products. These results highlight the potential usefulness of these pump-probe measurements as a tool to study conformer-specific dynamics in molecules of biological interest.

Keywords: strong field ionization; nonadiabatic dynamics; conical intersections; excited states; radical cation; conformers



Citation: Singh, V.; López Peña, H.A.; Shusterman, J.M.; Vindel-Zandbergen, P.; Tibbetts, K.M.; Matsika, S.

Conformer-Specific Dissociation Dynamics in Dimethyl Methylphosphonate Radical Cation. *Molecules* **2022**, *27*, 2269. <https://doi.org/10.3390/molecules27072269>

Academic Editor: Jianzhang Zhao

Received: 23 February 2022

Accepted: 28 March 2022

Published: 31 March 2022

Publisher's Note: MDPI stays neutral with regard to jurisdictional claims in published maps and institutional affiliations.



Copyright: © 2022 by the authors. Licensee MDPI, Basel, Switzerland. This article is an open access article distributed under the terms and conditions of the Creative Commons Attribution (CC BY) license (<https://creativecommons.org/licenses/by/4.0/>).

1. Introduction

Many photoinduced biological [1–3] and chemical [4,5] processes require the understanding of nuclear and electronic dynamics which occur on nanosecond to attosecond time scales. Ultrafast pump-probe spectroscopy [6] has been an effective experimental technique to study the dynamics occurring on an ultrafast time scale. In particular, strong field ionization followed by dissociation has been a useful technique to probe ultrafast dynamics in radical cations [7–12]. The pump pulse here ionizes molecules to create radical cations, whose dynamics are then studied with the help of a weak probe pulse that can excite to higher electronic states of the cation to induce dissociation.

One of the challenges in strong field ionization is to prepare a well-defined coherent state in the radical cation without excessive molecular fragmentation [12,13]. Strong field ionization often creates a superposition of electronic states in the cation, leading to a high probability that multiple fragmentation pathways will be accessed to form different fragments in an uncontrolled manner. However, strong-field ionization at laser wavelengths in the near-infrared region (~1200–1600 nm) can prepare a well-defined initial coherent state [9,13–15]. In the limit of adiabatic ionization, the strong field allows an electron to tunnel out through a Coulombic barrier, forming the parent cation on the ground electronic state, significantly reducing the number of fragmentations [14,16]. Adiabatic ionization is often described in terms of the Keldysh parameter (γ) [17], defined as the

frequency of incident laser pulse divided over the electron tunneling frequency. When the laser frequency is sufficiently low, γ is less than 1 and adiabatic ionization occurs primarily through tunneling, as is evidenced experimentally by less fragmentation [9,13,14]. Higher laser frequency (shorter wavelength), on the other hand, results in γ greater than 1 where tunneling is diminished, leading to non-adiabatic ionization and high degree of fragmentation.

Preparation of radical cations in their ground state via adiabatic ionization has led into a number of interesting observations of ion yield oscillations arising from the initial coherent vibrational dynamics. Levis and coworkers observed that coherent ion yield oscillations in acetophenone cation lasted 100 fs longer and were six times amplified when acetophenone was ionized adiabatically at 1270 nm as compared to ionizing nonadiabatically at 800 nm [9,18]. The antiphase oscillations between the parent acetophenone and fragment benzoyl cations with 650 fs period were attributed to coherent motion along the phenyl-acetyl twisting coordinate. Similar coherent twisting motions upon adiabatic ionization have been observed in other aromatic molecules including azobenzene [19], nitrobenzene [20], and nitrotoluenes [11,21,22]. There are many such instances where adiabatic ionization improved the amplitudes and lifetimes of oscillations in the ion signals of parent cation and secondary fragments, which provided better insight into the dynamics [12].

In recent studies one of us applied adiabatic ionization on dimethyl methylphosphonate (DMMP, $\text{PO}_3(\text{CH}_3)_3$) [13,23]. DMMP is a well-known simulant for organophosphorus chemical warfare agents, such as sarin and soman [24,25]. These nerve agents can lead to nerve paralysis and sometimes even death. Hence, having control schemes through which these molecules can be destructed might be helpful in detection of these agents. The experiment used near-infrared (1200 nm or 1500 nm) and 800 nm pump pulses to ionize DMMP adiabatically and non-adiabatically, respectively. Adiabatic ionization prepared a well-defined coherent vibrational state along the P=O stretching coordinate in the radical cation, resulting in high-amplitude ion yield oscillations with a period of 45 fs. The two major fragment ions, $\text{PO}_2\text{C}_2\text{H}_7^+$ and PO_2CH_4^+ , oscillate with the same period as the parent ion but with a phase shift of approximately π . These antiphase oscillations were attributed to electronic excitation of the parent ion by the 800 nm probe pulse, but no specific excitation pathways were identified.

Determining specific excitation pathways in DMMP^+ is complicated by the fact that DMMP, like many molecules, is present at room temperature as multiple rapidly converting conformational isomers, or conformers. Conformer-specific ionization and reaction dynamics have been observed in many molecules through spectroscopic excitation over the last two decades [26–33]. Most of these studies first separate distinct conformers spectroscopically or electrostatically before probing their individual dynamics and reactions [26–30], although more recently advanced techniques including Coulomb explosion imaging [31] and ultrafast electron diffraction [32,33] have distinguished structures and reaction dynamics of multiple conformers without prior separation. However, the potential for conformer-specific coherent vibrational dynamics to result in distinct excitation and dissociation pathways remains unexplored.

In this work, we use computational studies in an effort to better understand and interpret the dynamics observed by pump-probe spectroscopy on DMMP^+ , including the different conformers that are expected to be present. Trajectory surface hopping used to obtain the dynamics of the prepared cationic states reproduces the oscillatory behavior seen experimentally. High level coupled cluster calculations are also used to calculate higher cationic states that can be accessed with the probe laser, which clarifies specific features of the pump-probe signals in different fragmentation products. A comparison between a 800 nm and a 400 nm probe is also made providing further insight into the dynamics of DMMP^+ . The combination of the theoretical and experimental work offers a detailed description of the overall dynamics, and sheds light into how the excited state dynamics of different conformers can affect fragmentation.

2. Methods

2.1. Electronic Structure Calculations

All the geometries were optimized using Density Functional Theory (DFT) [34,35] with the B3LYP [36–39] functional and the 6-311+G(d) [40–44] basis set available in Gaussian 09 suite of packages [45]. Several conformers were optimized using initial structures reported previously, and were reoptimized in the current work for consistency [46]. Only two of these conformers are present at the experimental conditions, as will be discussed later. One of these conformers has C_s symmetry while the other one has no symmetry and will be denoted as C_1 . The neutral and the cationic geometries refer to the ground state minima of the neutral DMMP (S_0 minimum) and the radical cation DMMP⁺ (D_0 minimum) respectively. The single ionization potentials (IPs) of neutral DMMP were calculated at these optimized geometries at the EOM-IP-CCSD/6-311+G(d) level of theory. The IP calculations were also repeated with larger Dunning's correlation consistent basis set cc-pVTZ [47,48] to check the accuracy of the 6-311+G(d) results. Results are compared in Supplementary Material (SM) (Table S2), and confirm the accuracy of the 6-311+G(d) basis set.

In order to estimate the potential energy surfaces connecting the optimized neutral and cationic geometries, linear interpolations in all internal coordinates (LIIC) were done with 5 geometries connecting the initial and final geometries. Excited state energies and oscillator strengths of the transitions from the ground state (D_0) to the four excited states of DMMP cation were then calculated along the LIIC paths using EOM-EE-CCSD/6-311+G(d), CASSCF and EOM-IP-CCSD/6-311+G(d). In order to calculate the oscillator strengths from the first excited state to the higher states, the multi-reference method CASSCF [49] with an active space of 13 electrons in 9 orbitals and averaged over 7 states (7SA-CAS(13,9)) was used. For the active space of CASSCF, the P=O π orbitals and the lone pairs of oxygens were included. The orbitals are shown in SM (Figures S6 and S7). The active space was chosen by performing initial benchmarking studies to determine the best active space able to describe the first 5 IP states (See SM, Table S3). These CASSCF calculations were done with 6-311+G(d) basis set.

Conical intersections (CoIns) between cationic states, D_1/D_2 and D_2/D_3 , were calculated in order to explore pathways that facilitate radiationless decay after the probe excites population to higher states. Minimum points on the seam of CoIns were optimized using 5SA-CASSCF(13,9) with the 6-311G(d) basis set. We had to reduce the average of states from 7 to 5 and remove the diffuse functions because it was difficult to converge the calculations. The COLUMBUS software was used for the optimizations [50–52]. Because of the flexibility of the molecule it was not always possible to converge at the minimum of the seam. In that case we considered geometries on the seam (degenerate energies) even if the minimum was not reached. The energies at these geometries were recalculated using EOM-IP-CCSD/6-311+G(d).

Formation of two major fragments observed experimentally with m/z ratio 94 and 79 atomic mass require a hydrogen transfer step before fragmentation can occur. For this reason we calculated a pathway for the hydrogen transfer process. The optimized geometry of the tautomer produced from hydrogen transfer (denoted as HT) and the transition state connecting it to minimum of the ground state of DMMP⁺ (denoted as TS_{HT}) were optimized using B3LYP/6-311+G(d). The pathway connecting the conical intersections to TS_{HT} was calculated using a LIIC and calculating the energies of the five ionic states at the EOM-IP-CCSD/6-311+G(d) level of theory. These LIIC provide a path after the probe excitation to reach the intermediate HT which is needed for fragmentation to occur.

All CCSD calculations were done using Q-Chem suite of packages [53], while CASSCF calculations were performed using MOLPRO suite of packages [54]. The conical intersection searches were performed using COLUMBUS [50–52].

2.2. Dynamics

Generally, the strong field adiabatic ionization populates the ground state of the radical cation but since the first two IPs at S_0 geometry are very close, there is a high

probability of the first excited state of DMMP⁺ (D_1) to get populated along with D_0 by the pump laser. Hence, the dynamics on both of the states were studied using Trajectory Surface Hopping (TSH) [55,56]. We initially tested the behavior of the two dominant conformers by performing dynamics for both of them using one trajectory with zero initial momentum in each case. The results are shown in SM (Figure S20), and they demonstrate that the dynamics are very similar between the two conformers. Specifically, the main P=O vibration governing the oscillations on D_0 is identical for the two conformers. This is expected given the fact that the vibrational frequency for that mode is very similar for the two conformers (771 and 726 cm^{-1} for C_s and C_1 conformers, respectively). For this reason the subsequent dynamics, where we use many trajectories for a statistically significant picture, were performed only on one of the conformers, the C_1 .

To mimic the wave packet at $t = 0$ fs (when DMMP is ionized), 100 initial geometries (initial conditions) and their kinetic energies were generated around the S_0 minimum of the C_1 DMMP using a harmonic oscillator Wigner distribution, as implemented in Newton-X [57]. Wigner distribution requires the S_0 geometry and its normal modes to create these initial conditions; normal modes were calculated at the DFT level with the B3LYP functional and 6-311+G(d) basis set. The initial conditions were then propagated along the D_0 and D_1 potential energy surfaces (PESs) semiclassically: nuclei motions were treated classically with Newton's equations of motion whereas electronic energies, gradients of PES along which these geometries evolved, and non-adiabatic couplings in between the surfaces were treated quantum mechanically. The velocity-verlet algorithm was used to deal with nuclear motion with a time step of 0.5 fs. Electronic energies, gradients and non-adiabatic couplings were calculated on-the-fly using a 2 states averaged CASSCF, (2SA-CAS(13,9))/6-311G(d) using COLUMBUS [50–52]. The same set of active space orbitals were used for CASSCF as prescribed in Section 2.1 above. The Fewest Switches Surface Hopping (FSSH) algorithm [58], as implemented in Newton-X 2.2 [59], was used to consider the hopping between electronic surfaces. The dynamics were run for 200 fs. In order to conserve the total energy after a hop, the momentum vector of the nuclei was re-scaled along the derivative coupling vector. To deal with the decoherence of the wave functions after a hop, the Persico and Grannuci approach [60] was used, with the suggested decoherence factor of 0.1 Hartree [61]. Also, the trajectories were killed when the total energy deviated by 0.5 eV or more when compared with the total energy at the previous time step or at the time $t = 0$ fs.

2.3. Experimental Methods

The pump-probe experimental setups have been described in detail in our previous work [22,62]. Briefly, DMMP (Sigma-Aldrich) introduced into the vacuum chamber of a time-of-flight mass spectrometer was ionized with a 1300 nm, 20 fs, $8 \times 10^{13} \text{ W cm}^{-2}$ pump pulse. Separate measurements with two different probe pulses were performed. The first measurement with 800 nm, 35 fs, $8 \times 10^{12} \text{ W cm}^{-2}$ probe pulses and a time step of 3 fs used the setup described in Ref. [62]. The second measurement with 400 nm, 70 fs, $4 \times 10^{12} \text{ W cm}^{-2}$ pulses and a time step of 10 fs used the setup described in Ref. [22].

3. Results

3.1. Experimental Motivation

Pump-probe measurements on DMMP with strong-field adiabatic ionization at 1300 nm were taken using probe pulses at both 800 nm and 400 nm. Here, we focus on the time-dependent yields of the parent DMMP⁺ ion and the two major fragments $\text{PO}_2\text{C}_2\text{H}_7^+$ (m/z 94) and PO_2CH_4^+ (m/z 79). Previous mass spectrometry studies have established that $\text{PO}_2\text{C}_2\text{H}_7^+$ is produced directly from DMMP⁺ and that PO_2CH_4^+ is formed from secondary dissociation of $\text{PO}_2\text{C}_2\text{H}_7^+$ [63]. The pump-probe results for DMMP using 800 nm probe are shown in Figure 1a. The approximately antiphase ion yield oscillations between the parent DMMP⁺ and fragments $\text{PO}_2\text{C}_2\text{H}_7^+$ and PO_2CH_4^+ have been attributed to coherent excitation of the P=O stretching mode [13]. Moreover, the ion signal of DMMP⁺ substan-

tially depletes to $\sim 70\%$ of its negative delay value at around 100 fs, after which the signal increases to $\sim 84\%$ of its original value within 800 fs. Both the oscillations and slower dynamics of the DMMP^+ signal were observed in our earlier work [13,23]. The second measurement with 400 nm, 70 fs, $4 \times 10^{12} \text{ W cm}^{-2}$ pulses and a time step of 10 fs used the setup described in Ref. [22]. The transient ion signals from this measurement shown in Figure 1b do not exhibit the oscillations seen in Figure 1a because the long duration of the 400 nm probe pulse (70 fs) arising from frequency-doubling cannot resolve the coherent oscillations. Moreover, the DMMP^+ signal rapidly depletes to $\sim 80\%$ of its original value by 100 fs and remains constant thereafter, in contrast to the increase of DMMP^+ signal over 800 fs seen with the 800 nm probe.

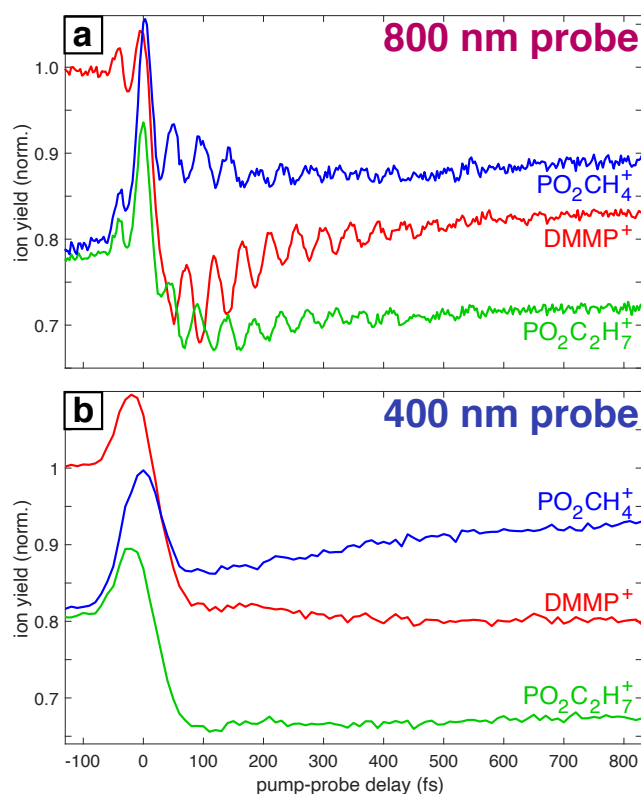


Figure 1. Transient ion signals of DMMP^+ (red), $\text{PO}_2\text{C}_2\text{H}_7^+$ (green), and PO_2CH_4^+ (blue) taken with (a) 800 nm and (b) 400 nm probe pulses.

To isolate the oscillatory dynamics seen in Figure 1a, the dynamics at >50 fs delays were fit to a series of decaying exponential functions as described in ref. [23]. In DMMP^+ , the two decay times of (19 ± 9) fs and (177 ± 13) fs extracted from the incoherent dynamics (i.e., not associated with oscillations) may be associated with electronic relaxation. However, we cannot assign these time scales to any specific pathway because only the D_0 and D_1 dynamics were studied theoretically in this work. Subtracting off these incoherent dynamics isolates the oscillatory dynamics shown in Figure 2. In our previous work using 5 fs time steps, we reported that oscillations in the fragment ion yields were out of phase with the DMMP^+ oscillations [13,23]. The present measurements taken with finer 3 fs time steps clearly show that the delays corresponding to the minima of the DMMP^+ oscillations, highlighted with the dotted lines in Figure 2, do not *exactly* match the delays associated with maximum $\text{PO}_2\text{C}_2\text{H}_7^+$ or PO_2CH_4^+ yields. Specifically, the $\text{PO}_2\text{C}_2\text{H}_7^+$ maximum (green) appears slightly ahead of the DMMP^+ minimum (red) and the PO_2CH_4^+ maximum (blue) appears slightly behind (Figure 2, top). To quantify these slight phase shifts, the oscillatory signals were fit to exponentially decaying cosine functions (Figure 2, bottom). The extracted oscillation phases of the $\text{PO}_2\text{C}_2\text{H}_7^+$ and PO_2CH_4^+ yields differ by 0.5 radians, or about 8%. Their phases relative to the DMMP^+ yield are 2.7 radians for $\text{PO}_2\text{C}_2\text{H}_7^+$ and

3.2 radians for PO_2CH_4^+ , demonstrating that neither fragment oscillates exactly out of phase (π radians) with DMMP^+ . This result could suggest distinct DMMP^+ geometries preferentially dissociate into $\text{PO}_2\text{C}_2\text{H}_7^+$ or PO_2CH_4^+ upon excitation at 800 nm.

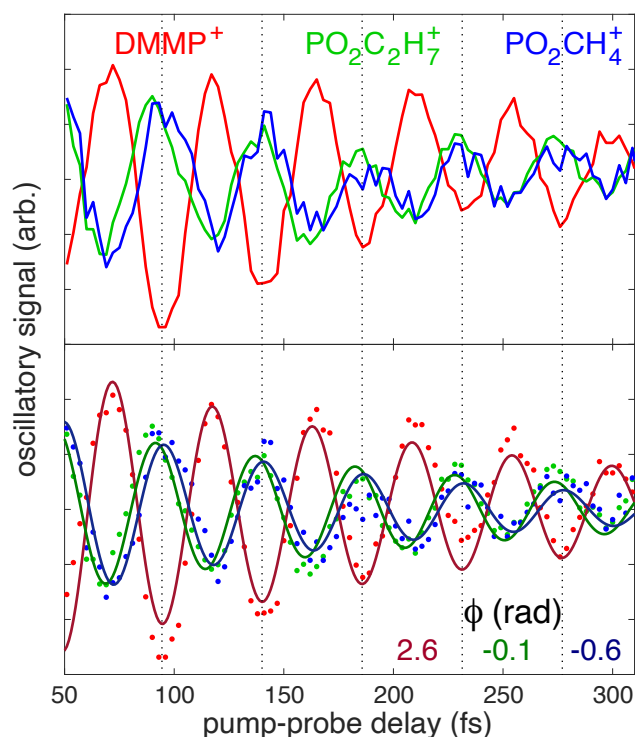


Figure 2. Oscillatory ion signals of DMMP^+ (red), $\text{PO}_2\text{C}_2\text{H}_7^+$ (green), and PO_2CH_4^+ (blue), shown as raw signals (**top**) and fit to exponentially decaying cosine functions (**bottom**). The extracted phases for each signal are shown; all signals had an oscillation period of 45.5 fs.

3.2. Ionization Potentials

In order to understand the underlying dynamics of the DMMP cation we performed a series of computations, starting from the ionization energies to produce the cation in its various electronic states. Several conformers of DMMP and its cation have been reported before [46,64]. The conformers of neutral DMMP and their associated relative energies are shown in SM (Figure S3). Based on their energies, only two of them are expected to be present at the experimental conditions, while the others are expected to be approximately 2% present. The major distinction between these two nearly isoenergetic conformers can be made based on the two 'O=P-O-C' dihedral angles which are equal for one case leading to C_s symmetry, but vary by approximately 25° for the other. The neutral equilibrium structures are denoted S_{0,C_s} and S_{0,C_1} , respectively throughout the text (See Figure 3).

Figure 3 shows ionization potentials (IPs) to several cationic states calculated for both conformers. The first two states, D_0 and D_1 , are almost degenerate, especially for the C_1 conformer. This is because of the character of the two states, which is shown in the figure by their Dyson orbitals. The two states originate by ionization of an electron in orbitals located along the P=O bond, and there are two such orbitals in perpendicular planes. This explains why these two states are very close in energy and they behave very similarly, in consequence this will play an important role during the dynamics to be discussed next. Above D_0 and D_1 there are four additional states which are almost equally separated by about 1 eV from each other. The variation of these states as the molecule relaxes to the D_0 minimum will play an important role in the observed pump probe behavior. The Dyson orbitals describing these states are shown in SM (Figures S4 and S5).

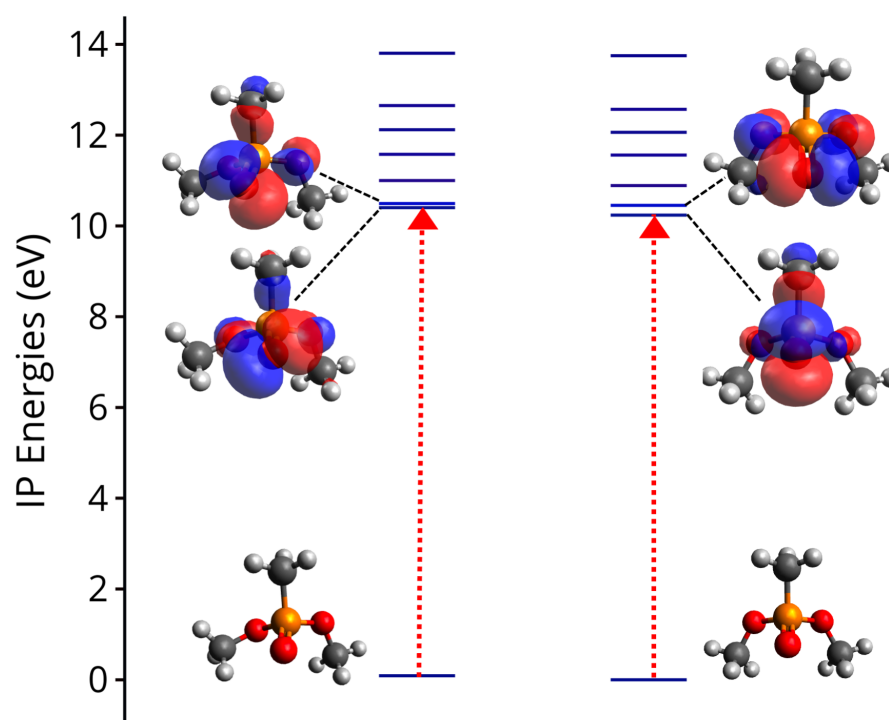


Figure 3. Vertical ionization potentials (IPs) of DMMP calculated at the EOM-IP-CCSD/6-311+G(d) level of theory for the C_1 conformer (S_{0,C_1} geometry, **left**) and C_s conformer (S_{0,C_s} geometry, **right**). All energies are in eV and are plotted with respect to S_{0,C_s} energy. The Dyson orbitals characterizing the hole of the first two cationic states are also shown, while the Dyson orbitals for the other states are shown in SM (Figures S4 and S5).

3.3. Dynamics on D_0 and D_1

Generally, strong field adiabatic ionization creates a substantial population of a radical cation on its ground state [9]. However, for DMMP since the first two cationic states (D_0 and D_1) are almost degenerate, the probability of ionizing to D_1 along with the ground state of $DMMP^+$, D_0 , is high. Hence, to understand the dynamics after ionization, both the D_0 and D_1 states have to be considered. As mentioned in Section 2, we only show results for 200 trajectories run using the C_1 conformer here. Comparisons for one trajectory between the C_s and C_1 conformer are shown in SM (Figure S20), demonstrating very similar behavior. Figure 4 shows the main results from two different sets of dynamics, one where all the population is on D_1 (Dyn_ D_1) and one with all the population on D_0 (Dyn_ D_0). The mean energies of D_0 and D_1 for all the trajectories initially populated on D_0 (Dyn_ D_0) or D_1 (Dyn_ D_1) are shown plotted versus time in Figure 4a. In Figure 4b the mean P=O bond length versus time for both sets of trajectories is shown. We plot the P=O bond length vs time because this is a main distortion going from the neutral geometry to the relaxed D_0 minimum, so this internal coordinate is a main evolving coordinate during the dynamics. This is also apparent by the nature of the orbital describing the unpaired electron which involves the P=O π bond for both D_0 and D_1 (Figure 3).

We first observe that the energies and P=O bond lengths for the two states D_0 and D_1 are parallel to each other for both sets of trajectories. This indicates that the potential energy surfaces of the states are parallel to each other and behave exactly the same way, so the dynamics observed are not affected by the fact that both states are populated. When the population starts in D_1 there is fast decay to D_0 (as shown in SM, Figure S17), but the nonadiabatic transitions do not affect the dynamics, as is clear from the oscillation of the P=O bond.

The most important observation is that the P=O bond length has an oscillatory behavior with time with a period of approximately 40 fs. Once the $DMMP^+$ cation is created

populations on either D_0 or D_1 oscillate along the P=O stretch with the time period of 40 fs. This period is very similar to the experimentally observed period in the fragments, and as will be discussed below is responsible for the experimental oscillations.

The fact that there are two conformers may complicate the dynamics, especially if conversion between them is observed. The barrier to convert between them is only 0.14 eV (see SM, Figure S12). In the dynamics however, we did not observe any meaningful conversion. Only two out of the total 200 trajectories converted from C_1 to the C_s conformer during the dynamics. Figure S19 in the SM demonstrates this by showing the average of the two dihedral angles C-O-P-O, which never become equal (as they should be in the C_s conformer). This suggests that the C_1 conformer remains asymmetric during the dynamics and similar behavior should be expected from the dynamics of the C_s conformer.

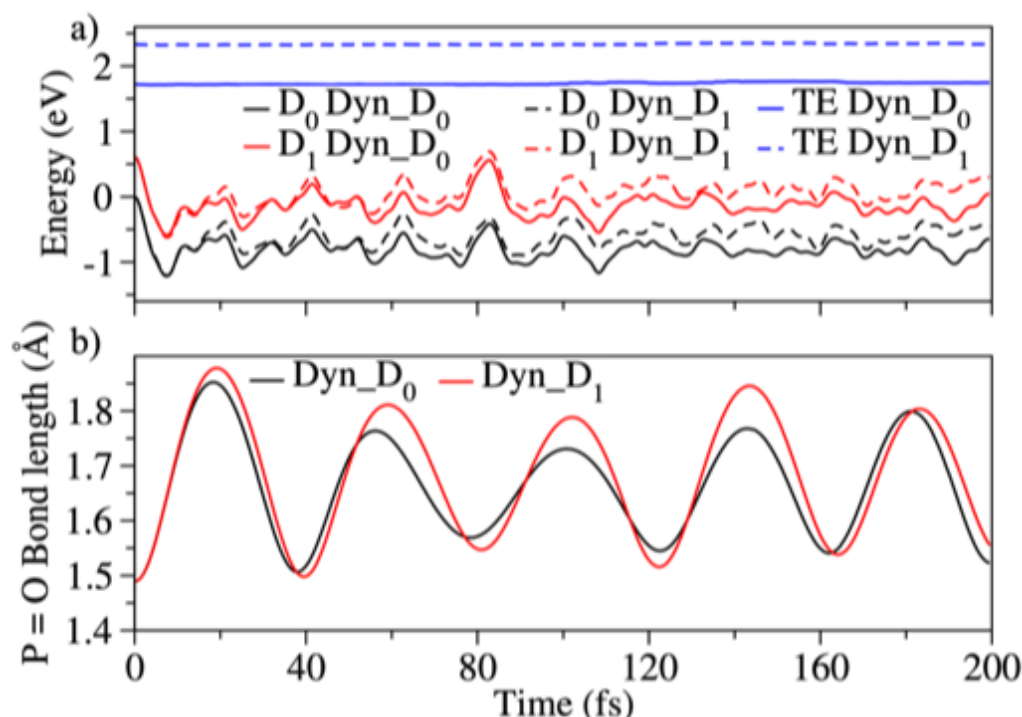


Figure 4. (a) Mean potential energies of D_0 , D_1 and the total energies (TE) plotted vs time for the dynamics of the populations starting on the electronic states D_0 (Dyn_ D_0) and D_1 (Dyn_ D_1). The energies were calculated on-the-fly using 2SA-CAS(13,9)/6-311G(d) level of theory. (b) Mean P=O bond lengths plotted vs time for the dynamics starting on D_0 or D_1 .

3.4. Effect of the Probe: Accessing Higher Electronic States

Using the results from the dynamics we can explain how the probe is responsible for the oscillatory behavior in the ion signals of the parent cation and the secondary fragments. Once DMMP⁺ is formed due to the pump pulse, the wavepacket oscillates on D_0 and D_1 with the time period of about 40 fs. The probe pulse then excites the population either from D_0 or D_1 to the higher electronic excited states depending on certain conditions: the energy gap between D_0 or D_1 and higher states has to be resonant with the probe energy, and the oscillator strength between the resonant states has to be non-negligible. To get a better picture of which excited states are populated by the probe we calculated the PES of several electronic states along the oscillatory coordinate. In Figure 5 the energies of several states are plotted along the geometries generated with linear interpolation connecting the neutral geometry (corresponding to vertical ionization) to the minimum of the cation. Since, there was no evidence of conversion between the C_1 and C_s conformers in the dynamics, we use LIICs connecting the C_1 neutral minimum geometry (S_{0,C_1}) to C_1 D_0 minimum geometry of the cation (D_{0,C_1}) and the C_s neutral minimum geometry (S_{0,C_s}) to the C_s D_0 minimum geometry (D_{0,C_s}) separately. The results at the EOM-IP-CCSD level are shown in Figure 5a,b, for C_1 and C_s , respectively, while similar plots at the CASSCF and EOM-

EE-CCSD level are shown in SM (Figures S8 and S9). The oscillator strengths along the LIICs are plotted in Figure 5c,d, for the C_1 and C_s conformers, respectively. Oscillator strengths are taken from the CASSCF calculations since EOM-IP-CCSD cannot calculate them between pairs of cationic states.

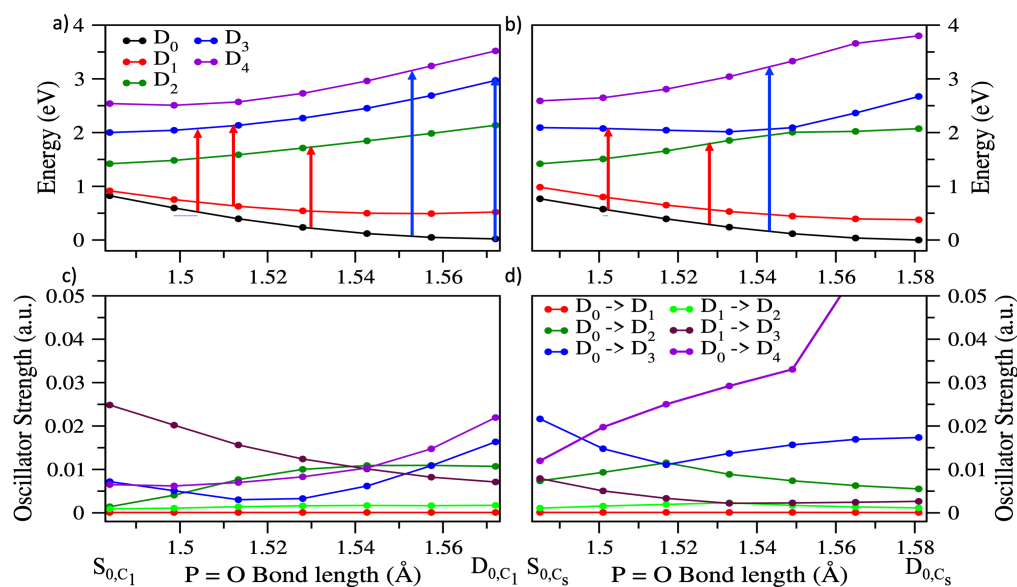


Figure 5. Energies along LIIC connecting vertical ionization to the minimum of the cation for (a) the asymmetric conformer, connecting the neutral minimum geometry, (S_{0,C_1}) to the cation minimum geometry (D_{0,C_1}); (b) the symmetric conformer, connecting the neutral minimum geometry (S_{0,C_s}) to the cation minimum geometry (D_{0,C_s}). The transitions due to probe light of 400 nm (3.1 eV) and 800 nm (1.6 eV) are represented with blue and red arrows respectively. (c,d) Oscillator strengths along the paths shown in (a,b), respectively. The vertical energies were calculated at the EOM-IP-CCSD/6-311+G(d) level of theory. The oscillator strengths were calculated at the 7SA-CASSCF(13,9)/6-311+G(d) level of theory.

The electronic excited states that are accessible due to probe light are shown with red and blue single headed arrows representing the 800 nm (1.55 eV) and 400 nm (3.10 eV) probes, respectively. First, we discuss the effects of 800 nm probe light which leads to oscillations in the ion signals of the radical cations. For the 800 nm probe, the accessible states based on both the energy gaps and oscillator strengths are D_2 or D_3 for both conformers, as can be seen in Figure 5a,b. These transitions can cause depletion in $DMMP^+$ population through dissociation into the observed fragments. Hence, the minima in the oscillation of $DMMP^+$ ion signal occur at roughly the same time as the maxima in the ion signals of $PO_2C_2H_7^+$ and $PO_2CH_4^+$ after every 40 fs. Experimentally, the time period of these oscillations is 45 fs (Figure 1) accounting for the relative error of our calculations to be 11%. This error is most likely due to the electronic structure. The CASSCF method that we used does not include dynamical correlation, so the structures and vibrational frequencies predicted are not very accurate. Errors in vibrational frequencies will directly affect the oscillation time.

With the 400 nm probe the higher energy states D_3 and D_4 can be accessed from D_0 as shown by the blue arrows in Figure 5a,b. Also, the oscillator strengths for these transitions are comparatively higher than for the 800 nm transitions. Since multiple electronic states are accessible and the probe light of 400 nm provides extra energy, different pathways could be accessed. The excited states can dissociate into many other secondary fragments observed in higher yields in the mass spectrum at +800 fs delay with the 400 nm probe (SM Figure S1). Moreover, the resonance of the 400 nm probe with allowed transitions to D_3 and D_4 at geometries close to D_{0,C_1} and D_{0,C_s} is consistent with the continued depletion of the $DMMP^+$ signal and increase in $PO_2CH_4^+$ at a time delay of +800 fs for the 400 nm probe seen in Figure 1. In contrast, the lack of resonant transitions with the 800 nm probe

near the D_{0,C_1} and D_{0,C_s} geometries explains the observed increase in intact DMMP⁺ signal with the 800 nm probe as the delay increases from 100 to 800 fs.

3.5. Differences between $PO_2CH_4^+$ and $PO_2C_2H_7^+$: Conformational Effects

Based on the previous discussion we expect that the fragments $PO_2CH_4^+$ and $PO_2C_2H_7^+$ are generated after probe excitations to D_2 and D_3 when the population of the parent ion is depleted. The oscillatory behaviors of these fragments in Figure 2 however are not completely in phase with one another. There is a small shift between them with $PO_2C_2H_7^+$ appearing slightly earlier than $PO_2CH_4^+$. According to our theoretical results there are two sources that can lead to this difference. The first hypothesis is that the different fragments are associated with excitation to separate excited states. According to Figure 5, the D_3 state can be accessed at shorter P=O bond lengths, which would imply that excitation to D_3 leads to $PO_2C_2H_7^+$ and excitation to D_2 leads to $PO_2CH_4^+$. The second hypothesis is that the different conformers, C_1 and C_s , are responsible for the two different fragments.

In order to test these hypotheses we need to examine the dynamics leading to dissociation. The dynamics should either be different between the two excited states or between the two conformers. The most likely pathway for fragmentation is that internal conversion to the ground state converts the electronic energy to extra vibrational energy which can be used to break bonds. Internal conversion should be very fast because of the close proximity of the states. Hence, after the probe excitation, the population on D_3 or D_2 will decay very fast to D_0 . Fast decay among cationic states has been calculated before for other systems [10], and is expected to be common in radical cations due to the high density of states. The radiationless transitions between pairs of states will lead to certain modes becoming vibrationally excited. In order to have a better idea of how the dynamics will proceed we calculated conical intersections between D_2/D_3 and between D_1/D_2 . The structures of these CoIns are shown in Figure 6. The main deformations occur along the two P-O bonds connected to the methyl groups. The third P=O bond that is responsible for the dynamics on D_0 and D_1 remains mostly unchanged at the initial value from vertical ionization of about 1.5 Å. Hence, any dynamics initiated by excitation to D_3 and D_2 will lead to vibrational excitation on the two P-O bonds. The branching vectors of the CoIns (shown in SM, Figure S13) show similarly that there is a lot of vibrational motion along the P-O bonds for both D_2/D_3 and between D_1/D_2 CoIns. These observations do not lead to any obvious differences between motion initiated on D_3 vs D_2 . On the other hand, there are some obvious differences between the C_s and C_1 geometries of the CoIns. In the C_s conformer the D_2/D_3 CoIn leads to a small contraction of the P-O symmetric bonds from their initial value of 1.62 Å to 1.57 Å. The D_1/D_2 CoIn though increases these bonds to 1.67 Å creating a vibrationally excited motion along these bonds. The C_1 conformer behaves the opposite way. The D_2/D_3 CoIn increases the P-O bonds to 1.67 Å while the D_1/D_2 CoIn leads to a very asymmetric structure with one bond contracted and the other extended significantly. So, in this structure it is more likely that vibrational excitation is mostly on one P-O bond. It is natural to expect then that this asymmetric deformation can easier lead to a fragmentation where only one P-O bond is broken (as in $PO_2C_2H_7^+$) while the C_s conformer with its symmetric expansion of the P-O bonds can lead to excess vibrational energy on both P-O bonds which can eventually lead to the sequential fragmentation producing $PO_2CH_4^+$.

Although these calculations provide a clear correlation between the two conformers and the two observed fragments, it is harder to explain the appearance of fragment $PO_2C_2H_7^+$ at slightly earlier times. This will depend on when exactly the gap between D_0 and D_3 matches the photon energy in the two conformers. The energy difference is very sensitive to the level of theory we are using, so we cannot be confident that we can resolve very small changes. On the other hand, the different behavior of the D_3 state between the two conformers that can lead to different fragments is observed at all levels of theory we used. As seen in Figure 5 the slope of D_3 is very different in the two conformers, with D_3 increasing in energy along the oscillations in the asymmetric conformer and decreasing in

the symmetric conformer. This is also observed using CASSCF and EOM-EE-CCSD, as seen in SM (Figures S8 and S9). Overall, the calculations support with reasonable confidence the assignment that excitation of the C_1 conformer will lead to $\text{PO}_2\text{C}_2\text{H}_7^+$ while excitation of C_s leads to fragment PO_2CH_4^+ .

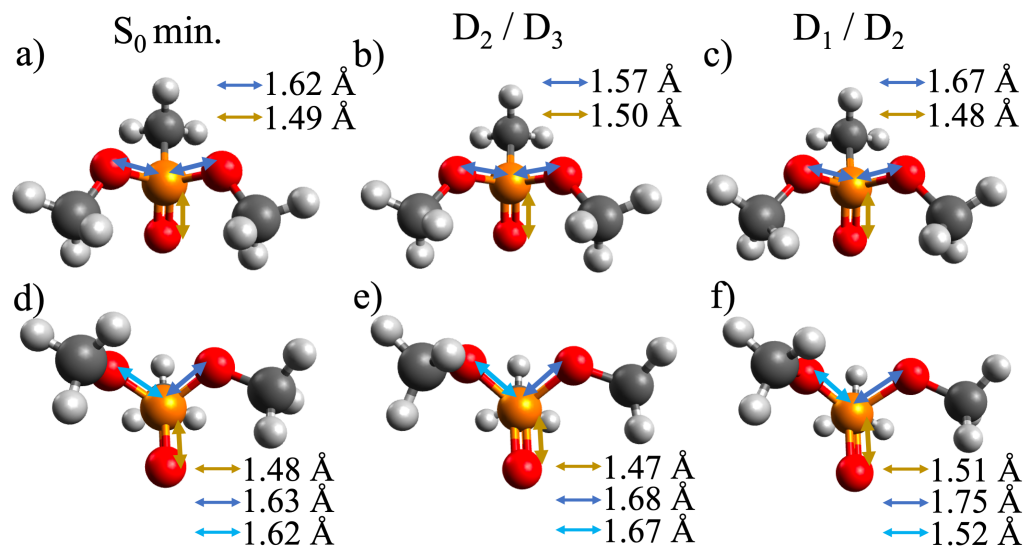


Figure 6. Structures of (a,d) S_{0,C_s} and S_{0,C_1} geometries, and the conical intersections between (b,e) D_2/D_3 and (c,f) D_1/D_2 states for the (b,c) C_s symmetric and (e,f) C_1 asymmetric conformers. CoIns structures are optimized at the CASSCF level. The three P-O bond lengths are shown in Å.

3.6. Hydrogen Transfer

Dissociation on the ground state to form the observed fragments $\text{PO}_2\text{C}_2\text{H}_7^+$ and PO_2CH_4^+ requires an initial hydrogen transfer step. In the HT isomer, one of the hydrogens from the oxymethyl group migrates to the oxygen attached to phosphorus. We have located a transition state on D_0 which can lead to this HT isomer (denoted TS_{HT}). This transition state is the same for both conformers and we have connected it to the HT conformer (SM Figure S14).

Figure 7 shows how TS_{HT} can be easily accessed after the probe excitation for both conformers. On the top side, it is shown that after the probe excites the cation to D_3 or D_2 , two CoIns D_2/D_3 and D_1/D_2 can be reached with the P-O bonds being the primary changing coordinates. On the bottom side of the figure, a LIIC connects the D_1/D_2 CoIn to TS_{HT} . It is obvious from these figures that TS_{HT} is accessed barrierlessly after internal conversion to D_1 . A CoIn between D_1 and D_0 occurs along this path as well, as can be seen in Figure 7. The pathway is barrierless for both conformers, although it appears more downhill for the C_s conformer. The steeper slope for the C_s conformer can be associated with more excess vibrational energy in that conformer that can further be used for sequential fragmentation to PO_2CH_4^+ , which requires approximately 1 eV more energy than fragmentation to $\text{PO}_2\text{C}_2\text{H}_7^+$ [64].

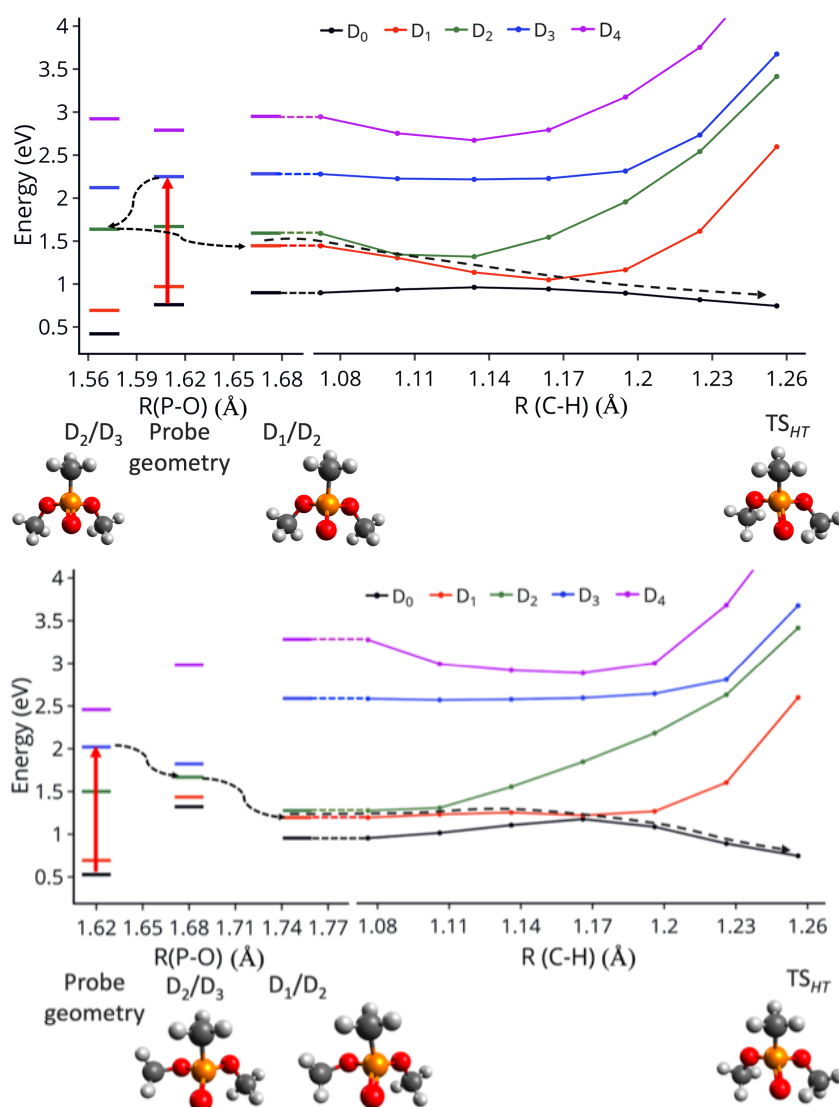


Figure 7. Top: Energies at the geometry of probe pulse excitation to D_3 ; at the CoIn D_2/D_3 geometry and at the CoIn D_1/D_2 geometry. **Bottom:** Energies along LIICs connecting the D_1/D_2 CoIn to the transition state (TS_{HT}). Top plots show the energies for the C_s conformer and bottom plots for the C_1 . All the calculations were done at EOM-IP-CCSD/6-311+G(d) level of theory.

4. Discussion

Conformationally selective dynamics are difficult to observe since it is often challenging to distinguish between conformers due to the small rotational barriers separating them. Nevertheless, the ubiquity and importance of conformers in chemistry and biology has inspired many experimental studies using a variety of techniques to observe conformation-specific chemistry [26–33]. In this work, we have observed that the two main conformers of $DMMP^+$ present in the experiment have distinct excited state dynamics while they behave very similarly in the ground state. The difference in the dynamics is governed by the different behavior of the excited states PES, which can channel vibrational energy in different ways for the two conformers. During internal conversion, the C_s conformer converts the electronic energy into vibrational energy along both P-O bonds symmetrically, while the C_1 conformer goes through an asymmetric vibrational motion along the two P-O bonds. Ultimately, the difference in the dynamics leads to different dissociation products, as evidenced in the experimental fragmentation dynamics. Specifically, the slight difference in the phases of the oscillations in the fragments $PO_2C_2H_7^+$ and $PO_2CH_4^+$ is evidence that they are initiated from different pathways.

The dynamics after the probe have been theoretically investigated here using static electronic structure calculations exploring the pathways, rather than dynamics. The most accurate theoretical study would require modeling of the dynamics after the probe excitation all the way to fragmentation to the two products. This process however is expected to take much longer than we are able to model with *ab initio* on the fly dynamics, especially since the fragmentation to PO_2CH_4^+ is sequential [63]. The static calculations however, combined with the experimental observations of the different oscillation phases for the two fragments, provide the most plausible explanation for the underlying dynamics. Moreover, the ability to observe small (8%, or about 4 fs) phase shifts in the ion signals of different fragments demonstrates the potential power of pump-probe measurements to observe and possibly control nuclear dynamics in different conformers. Hence, pump-probe measurements can provide a complementary ultrafast spectroscopy tool to Coulomb explosion imaging [31] and electron diffraction [32,33] to study conformer-specific dynamics in molecules of biological interest.

5. Conclusions

We have investigated the dynamics of the DMMP cation after production by strong field adiabatic ionization. The pump-probe results using 800 nm probe show oscillations in the parent DMMP^+ and fragments $\text{PO}_2\text{C}_2\text{H}_7^+$ and PO_2CH_4^+ that were previously attributed to coherent oscillations of the P=O stretching bond [13]. Here we examined the details of the dynamics using trajectory surface hopping calculations. The TSH results demonstrate that indeed after vertical ionization to either the ground state D_0 or the nearly isoenergetic first excited state D_1 , coherent oscillations along the P=O bond occur with a period of about 40 fs, very similar to the 45 fs observed experimentally. The probe pulse excites the cation to higher states D_2 and D_3 when it is resonant with the corresponding energy gap. Internal conversion from D_2 or D_3 can occur rapidly through conical intersections converting the electronic energy to vibrational energy further leading to dissociation.

The slight phase shift between the oscillations of the two fragment ions $\text{PO}_2\text{C}_2\text{H}_7^+$ and PO_2CH_4^+ observed in the pump-probe measurements was attributed to the presence of two main conformers of DMMP at experimental conditions. These conformers exhibit very similar dynamics after ionization, both of them oscillating along D_0 with a period of about 40 fs. Quite interestingly, however, the theoretical results show that the two conformers have very different dynamics after being excited by the probe pulse. They return to the ground state through different CoIns acquiring vibrational energy distributed differently among the internal degrees of freedom. Comparisons with the experimental observations indicate that the differences in the dynamics eventually lead to different fragments produced from the two conformers. Specifically, fragment $\text{PO}_2\text{C}_2\text{H}_7^+$ is expected to be produced from the C_1 conformer, which has excess vibrational energy mainly along one of the P-O bonds, while PO_2CH_4^+ can be produced sequentially after the production of $\text{PO}_2\text{C}_2\text{H}_7^+$ in the C_s conformer, which has both P-O bonds vibrationally excited after passing through CoIns. This combined experimental and theoretical study provides a unique example of conformer-specific dissociation dynamics, where conformers separated by very small energetic barriers can lead to different fragments, and indicates that these pump-probe measurements can provide a complementary ultrafast spectroscopy tool to study conformer-specific dynamics in molecules of biological interest.

Supplementary Materials: The following supporting information can be downloaded at: <https://www.mdpi.com/article/10.3390/molecules27072269/si>. Experimental information: mass spectra of DMMP ionized at 1300 nm pump with 400 nm and 800 nm probes. Theoretical information: geometries and energetics for all conformers; IPs at different geometries and levels of theory; orbitals; comparison of different levels of theory for pathways; details of conical intersections and the surface hopping dynamics; cartesian coordinates of stationary points.

Author Contributions: Experimental measurements and analysis, H.A.L.P., J.M.S. and K.M.T.; Computational calculations and analysis, V.S., P.V.-Z. and S.M.; Funding acquisition, S.M. and K.M.T.;

Writing—original draft preparation: V.S., S.M. and K.M.T.; Writing—review and editing, S.M., P.V.-Z., H.A.L.P. and K.M.T. All authors have read and agreed to the published version of the manuscript.

Funding: V.S. and S.M. acknowledge support by DOE Award No. DE-FG02-08ER15983. H.A.L.P., J.M.S., and K.M.T. acknowledge support from the U.S. Army Research Office through Contract W911NF-19-1-0099. HALP acknowledges the generous support of an Altria Graduate Research Fellowship. Part of the computational work was performed using the Extreme Science and Engineering Discovery Environment (XSEDE), which is supported by National Science Foundation Grant No. ACI-1548562.

Institutional Review Board Statement: Not applicable.

Informed Consent Statement: Not applicable.

Data Availability Statement: The data used for this study can be requested from the correspondence author.

Conflicts of Interest: The authors declare no conflict of interest.

References

1. Mathies, R.A. A coherent picture of vision. *Nat. Chem.* **2015**, *7*, 945–947. [[CrossRef](#)] [[PubMed](#)]
2. Crespo-Hernández, C.E.; Cohen, B.; Hare, P.M.; Kohler, B. Ultrafast excited-state dynamics in nucleic acids. *Chem. Rev.* **2004**, *104*, 1977–2020. [[CrossRef](#)]
3. Calegari, F.; Ayuso, D.; Trabattori, A.; Belshaw, L.; De Camillis, S.; Anumula, S.; Frassetto, F.; Poletto, L.; Palacios, A.; Decleva, P.; et al. Ultrafast electron dynamics in phenylalanine initiated by attosecond pulses. *Science* **2014**, *346*, 336–339. [[CrossRef](#)]
4. Attar, A.R.; Bhattacharjee, A.; Pemmaraju, C.; Schnorr, K.; Closser, K.D.; Prendergast, D.; Leone, S.R. Femtosecond X-ray spectroscopy of an electrocyclic ring-opening reaction. *Science* **2017**, *356*, 54–59. [[CrossRef](#)] [[PubMed](#)]
5. Haas, Y. Photochemical α -cleavage of ketones: Revisiting acetone. *Photochem. Photobiol. Sci.* **2004**, *3*, 6–16. [[CrossRef](#)] [[PubMed](#)]
6. Maiuri, M.; Garavelli, M.; Cerullo, G. Ultrafast spectroscopy: State of the art and open challenges. *J. Am. Chem. Soc.* **2019**, *142*, 3–15. [[CrossRef](#)] [[PubMed](#)]
7. Pearson, B.J.; Nichols, S.R.; Weinacht, T. Molecular fragmentation driven by ultrafast dynamic ionic resonances. *J. Chem. Phys.* **2007**, *127*, 131101. [[CrossRef](#)] [[PubMed](#)]
8. Bohinski, T.; Moore Tibbetts, K.; Tarazkar, M.; Romanov, D.; Matsika, S.; Levis, R. Measurement of ionic resonances in alkyl phenyl ketone cations via infrared strong field mass spectrometry. *J. Phys. Chem. A* **2013**, *117*, 12374–12381. [[CrossRef](#)]
9. Bohinski, T.; Moore Tibbetts, K.; Tarazkar, M.; Romanov, D.A.; Matsika, S.; Levis, R.J. Strong field adiabatic ionization prepares a launch state for coherent control. *J. Phys. Chem. Lett.* **2014**, *5*, 4305–4309. [[CrossRef](#)] [[PubMed](#)]
10. Assmann, M.; Weinacht, T.; Matsika, S. Surface Hopping Investigation of the Relaxation Dynamics in Radical Cations. *J. Chem. Phys.* **2016**, *144*, 034301. [[CrossRef](#)] [[PubMed](#)]
11. Ampadu Boateng, D.; Gutsev, G.L.; Jena, P.; Tibbetts, K.M. Dissociation dynamics of 3- and 4-nitrotoluene radical cations: Coherently driven C–NO₂ bond homolysis. *J. Chem. Phys.* **2018**, *148*, 134305. [[CrossRef](#)]
12. Moore Tibbetts, K. Coherent vibrational and dissociation dynamics of polyatomic radical cations. *Chem. Eur. J.* **2019**, *25*, 8431–8439. [[CrossRef](#)]
13. Boateng, D.A.; Gutsev, G.L.; Jena, P.; Tibbetts, K.M. Ultrafast coherent vibrational dynamics in dimethyl methylphosphonate radical cation. *Phys. Chem. Chem. Phys.* **2018**, *20*, 4636–4640. [[CrossRef](#)] [[PubMed](#)]
14. Lezius, M.; Blanchet, V.; Rayner, D.; Villeneuve, D.; Stolow, A.; Ivanov, M.Y. Nonadiabatic multielectron dynamics in strong field molecular ionization. *Phys. Rev. Lett.* **2001**, *86*, 51. [[CrossRef](#)] [[PubMed](#)]
15. Markevitch, A.N.; Romanov, D.A.; Smith, S.M.; Schlegel, H.B.; Ivanov, M.Y.; Levis, R.J. Sequential nonadiabatic excitation of large molecules and ions driven by strong laser fields. *Phys. Rev. A* **2004**, *69*, 013401. [[CrossRef](#)]
16. Tolstikhin, O.I.; Morishita, T. Adiabatic theory of ionization by intense laser pulses: Finite-range potentials. *Phys. Rev. A* **2012**, *86*, 043417. [[CrossRef](#)]
17. Keldysh, L. Ionization in the field of a strong electromagnetic wave. *Sov. Phys. JETP* **1965**, *20*, 1307–1314.
18. Tibbetts, K.M.; Tarazkar, M.; Bohinski, T.; Romanov, D.A.; Matsika, S.; Levis, R.J. Controlling the dissociation dynamics of acetophenone radical cation through excitation of ground and excited state wavepackets. *J. Phys. B At. Mol. Opt. Phys.* **2015**, *48*, 164002. [[CrossRef](#)]
19. Munkerup, K.; Romanov, D.; Bohinski, T.; Stephansen, A.B.; Levis, R.J.; Sølling, T.I. Conserving Coherence and Storing Energy during Internal Conversion: Photoinduced Dynamics of cis- and trans-Azobenzene Radical Cations. *J. Phys. Chem. A* **2017**, *121*, 8642–8651. [[CrossRef](#)] [[PubMed](#)]
20. Peña, H.L.; Boateng, D.A.; McPherson, S.; Tibbetts, K.M. Using computational chemistry to design pump-probe schemes for measuring radical cation dynamics. *Phys. Chem. Chem. Phys.* **2021**, *23*, 13338–13348. [[CrossRef](#)]
21. Ampadu Boateng, D.; Word, M.D.; Gutsev, L.G.; Jena, P.; Tibbetts, K.M. Conserved Vibrational Coherence in the Ultrafast Rearrangement of 2-Nitrotoluene Radical Cation. *J. Phys. Chem. A* **2019**, *123*, 1140–1152. [[CrossRef](#)] [[PubMed](#)]

22. Lopez Pena, H.A.; Shusterman, J.M.; Ampadu Boateng, D.; Lao, K.U.; Tibbetts, K.M. Coherent control of molecular dissociation by selective excitation of nuclear wave packets. *Front. Chem.* **2022**, *in press*. [[CrossRef](#)]
23. Ampadu Boateng, D.; Word, M.D.; Tibbetts, K.M. Probing Coherent Vibrations of Organic Phosphonate Radical Cations with Femtosecond Time-Resolved Mass Spectrometry. *Molecules* **2019**, *24*, 509. [[CrossRef](#)]
24. Zheng, Q.; Fu, Y.C.; Xu, J.Q. Advances in the chemical sensors for the detection of DMMP—A simulant for nerve agent sarin. *Procedia Eng.* **2010**, *7*, 179–184. [[CrossRef](#)]
25. Tomchenko, A.A.; Harmer, G.P.; Marquis, B.T. Detection of chemical warfare agents using nanostructured metal oxide sensors. *Sens. Actuators B Chem.* **2005**, *108*, 41–55. [[CrossRef](#)]
26. Park, S.; Kim, S.; Kim, M. Observation of conformation-specific pathways in the photodissociation of 1-iodopropane ions. *Nature* **2002**, *415*, 306–308. [[CrossRef](#)] [[PubMed](#)]
27. Khriachtchev, L.; Pettersson, M.; Rasanen, M. Conformational Memory in Photodissociation of Formic Acid. *J. Am. Chem. Soc.* **2002**, *124*, 10994–10995. [[CrossRef](#)]
28. Kim, M.H.; Shen, L.; Tao, H.; Martinez, T.J.; Suits, A.G. Conformationally Controlled Chemistry: Excited-State Dynamics Dictate Ground-State Reaction. *Science* **2007**, *315*, 1561. [[CrossRef](#)]
29. Chang, Y.P.; Długołęcki, K.; Küpper, J.; Rösch, D.; Wild, D.; Willitsch, S. Specific Chemical Reactivities of Spatially Separated 3-Aminophenol Conformers with Cold Ca⁺ Ions. *Science* **2013**, *342*, 98–101. [[CrossRef](#)] [[PubMed](#)]
30. Lee, H.; Kim, S.Y.; Lim, J.S.; Kim, J.; Kim, S.K. Conformer Specific Excited-State Structure of 3-Methylthioanisole. *J. Phys. Chem. A* **2020**, *124*, 4666–4671. [[CrossRef](#)]
31. Pathak, S.; Obaid, R.; Bhattacharyya, S.; Bürger, J.; Li, X.; Tross, J.; Severt, T.; Davis, B.; Bilodeau, R.C.; Trallero-Herrero, C.A.; et al. Differentiating and Quantifying Gas-Phase Conformational Isomers Using Coulomb Explosion Imaging. *J. Phys. Chem. Lett.* **2020**, *11*, 10205–10211. [[CrossRef](#)] [[PubMed](#)]
32. Wilkin, K.J.; Parrish, R.M.; Yang, J.; Wolf, T.J.A.; Nunes, J.P.F.; Guehr, M.; Li, R.; Shen, X.; Zheng, Q.; Wang, X.; et al. Diffractive imaging of dissociation and ground-state dynamics in a complex molecule. *Phys. Rev. A* **2019**, *100*, 023402. [[CrossRef](#)]
33. Champenois, E.G.; Sanchez, D.M.; Yang, J.; Nunes, J.P.F.; Attar, A.; Centurion, M.; Forbes, R.; Gühr, M.; Hegazy, K.; Ji, F.; et al. Conformer-specific photochemistry imaged in real space and time. *Science* **2021**, *374*, 178–182. [[CrossRef](#)]
34. Ziegler, T. Approximate density functional theory as a practical tool in molecular energetics and dynamics. *Chem. Rev.* **1991**, *91*, 651–667. [[CrossRef](#)]
35. Kohn, W.; Becke, A.D.; Parr, R.G. Density functional theory of electronic structure. *J. Phys. Chem.* **1996**, *100*, 12974–12980. [[CrossRef](#)]
36. Becke, A.D. Becke's three parameter hybrid method using the LYP correlation functional. *J. Chem. Phys.* **1993**, *98*, 5648–5652. [[CrossRef](#)]
37. Becke, A.D. Density-functional exchange-energy approximation with correct asymptotic behavior. *Phys. Rev. A At. Mol. Opt. Phys.* **1988**, *38*, 3098. [[CrossRef](#)] [[PubMed](#)]
38. Lee, C.; Yang, W.; Parr, R.G. Development of the Colle-Salvetti correlation-energy formula into a functional of the electron density. *Phys. Rev. B Condens. Matter Mater. Phys.* **1988**, *37*, 785. [[CrossRef](#)] [[PubMed](#)]
39. Vosko, S.H.; Wilk, L.; Nusair, M. Accurate spin-dependent electron liquid correlation energies for local spin density calculations: A critical analysis. *Can. J. Phys.* **1980**, *58*, 1200–1211. [[CrossRef](#)]
40. Clark, T.; Chandrasekhar, J.; Spitznagel, G.W.; Schleyer, P.V.R. Efficient diffuse function-augmented basis sets for anion calculations. III. The 3-21+G basis set for first-row elements, Li-F. *J. Comput. Chem.* **1983**, *4*, 294–301. [[CrossRef](#)]
41. Francl, M.M.; Pietro, W.J.; Hehre, W.J.; Binkley, J.S.; Gordon, M.S.; DeFrees, D.J.; Pople, J.A. Self-consistent molecular orbital methods. XXIII. A polarization-type basis set for second-row elements. *J. Chem. Phys.* **1982**, *77*, 3654–3665. [[CrossRef](#)]
42. McLean, A.D.; Chandler, G.S. Contracted Gaussian basis sets for molecular calculations. I. Second row atoms, Z=11–18. *J. Chem. Phys.* **1980**, *72*, 5639–5648. [[CrossRef](#)]
43. Krishnan, R.; Binkley, J.S.; Seeger, R.; Pople, J.A. Self-consistent molecular orbital methods. XX. A basis set for correlated wave functions. *J. Chem. Phys.* **1980**, *72*, 650–654. [[CrossRef](#)]
44. Spitznagel, G.W.; Clark, T.; Schleyer, P.V.R.; Hehre, W.J. An evaluation of the performance of diffuse function-augmented basis sets for second row elements, Na-Cl. *J. Comput. Chem.* **1987**, *8*, 1109–1116. [[CrossRef](#)]
45. Frisch, M.J.; Trucks, G.W.; Schlegel, H.B.; Scuseria, G.E.; Robb, M.A.; Cheeseman, J.R.; Scalmani, G.; V. Barone, G.A.P.; Nakatsuji, H.; Li, X.; et al. *Gaussian 09, Revision B. 01*; Gaussian, Inc.: Wallingford, CT, USA, 2009.
46. Yang, L.; Shroll, R.M.; Zhang, J.; Lourderaj, U.; Hase, W.L. Theoretical investigation of mechanisms for the gas-phase unimolecular decomposition of DMMP. *J. Phys. Chem. A* **2009**, *113*, 13762–13771. [[CrossRef](#)]
47. Dunning, T.H. Gaussian basis sets for use in correlated molecular calculations. I. The atoms boron through neon and hydrogen. *J. Chem. Phys.* **1989**, *90*, 1007–1023. [[CrossRef](#)]
48. Woon, D.E.; Dunning, T.H. Gaussian basis sets for use in correlated molecular calculations. III. The atoms aluminum through argon. *J. Chem. Phys.* **1993**, *98*, 1358–1371. [[CrossRef](#)]
49. Roos, B.O.; Taylor, P.R.; Sigbahn, P.E. A complete active space SCF method (CASSCF) using a density matrix formulated super-CI approach. *Chem. Phys.* **1980**, *48*, 157–173. [[CrossRef](#)]

50. Lischka, H.; Shepard, R.; Pitzer, R.M.; Shavitt, I.; Dallos, M.; Müller, T.; Szalay, P.G.; Seth, M.; Kedziora, G.S.; Yabushita, S.; et al. High-Level Multireference Methods in the Quantum-Chemistry Program System COLUMBUS: Analytic MR-CISD and MR-AQCC Gradients and MR-AQCC-LRT for Excited States, GUGA Spin-Orbit CI and Parallel CI Density. *Phys. Chem. Chem. Phys.* **2001**, *3*, 664–673. [[CrossRef](#)]
51. Lischka, H.; Shepard, R.; Müller, T.; Szalay, P.G.; Pitzer, R.M.; Aquino, A.J.A.; Araújo do Nascimento, M.M.; Barbatti, M.; Belcher, L.T.; Blaudeau, J.P.; et al. The generality of the GUGA MRCI approach in COLUMBUS for treating complex quantum chemistry. *J. Chem. Phys.* **2020**, *152*, 134110. [[CrossRef](#)]
52. Lischka, H.; Shepard, R.; Shavitt, I.; Pitzer, R.M.; Dallos, M.; Müller, T.; Szalay, P.G.; Brown, F.B.; Ahlrichs, R.; Böhm, H.J.; et al. COLUMBUS, an ab Initio Electronic Structure Program, Release 7.0 (2017). *Phys. Chem. Chem. Phys.* **2017**, *19*, 5888–5894.
53. Shao, Y.; Gan, Z.; Epifanovsky, E.; Gilbert, A.T.; Wormit, M.; Kussmann, J.; Lange, A.W.; Behn, A.; Deng, J.; Feng, X.; et al. Advances in molecular quantum chemistry contained in the Q-Chem 4 program package. *Mol. Phys.* **2015**, *113*, 184–215. [[CrossRef](#)]
54. Werner, H.J.; Knowles, P.J.; Manby, F.R.; Black, J.A.; Doll, K.; Heßelmann, A.; Kats, D.; Köhn, A.; Korona, T.; Kreplin, D.A.; et al. The Molpro quantum chemistry package. *J. Chem. Phys.* **2020**, *152*, 144107. [[CrossRef](#)]
55. Barbatti, M. Nonadiabatic dynamics with trajectory surface hopping method. *Wiley Interdiscip. Rev. Comput. Mol. Sci.* **2011**, *1*, 620–633. [[CrossRef](#)]
56. Tully, J.C. Perspective: Nonadiabatic dynamics theory. *J. Chem. Phys.* **2012**, *137*, 22A301. [[CrossRef](#)] [[PubMed](#)]
57. Barbatti, M.; Granucci, G.; Ruckebauer, M.; Plasser, F.; Crespo-Otero, R.; Pittner, J.; Persico, M.; Lischka, H. NEWTON-X: A Package for Newtonian Dynamics Close to the Crossing Seam. Version 2. Available online: www.newtonx.org (accessed on 22 February 2022).
58. Tully, J.C. Molecular dynamics with electronic transitions. *J. Chem. Phys.* **1990**, *93*, 1061–1071. [[CrossRef](#)]
59. Barbatti, M.; Granucci, G.; Ruckebauer, M.; Plasser, F.; Crespo-Otero, R.; Pittner, J.; Persico, M.; Lischka, H. NEWTON-X: A surface-hopping program for nonadiabatic molecular dynamics. *WIREs Comp. Mol. Sci.* **2014**, *4*, 96. [[CrossRef](#)]
60. Granucci, G.; Persico, M. Critical appraisal of the fewest switches algorithm for surface hopping. *J. Chem. Phys.* **2007**, *126*, 134114. [[CrossRef](#)] [[PubMed](#)]
61. Zhu, C.; Nangia, S.; Jasper, A.W.; Truhlar, D.G. Coherent switching with decay of mixing: An improved treatment of electronic coherence for non-Born–Oppenheimer trajectories. *J. Chem. Phys.* **2004**, *121*, 7658–7670. [[CrossRef](#)] [[PubMed](#)]
62. Boateng, D.A.; Tibbetts, K.M. Measurement of ultrafast vibrational coherences in polyatomic radical cations with strong-field adiabatic ionization. *J. Vis. Exp. JoVE* **2018**, *138*, e58263.
63. Holtzclaw, J.R.; Wyatt, J.R.; Campana, J.E. Structure and Fragmentation of Dimethyl Methylphosphonate and Trimethyl Phosphite. *Org. Mass Spectrom.* **1985**, *20*, 90–97. [[CrossRef](#)]
64. Gutsev, G.L.; Ampadu Boateng, D.; Jena, P.; Tibbetts, K.M. A Theoretical and Mass Spectrometry Study of Dimethyl Methylphosphonate: New Isomers and Cation Decay Channels in an Intense Femtosecond Laser Field. *J. Phys. Chem. A* **2017**, *121*, 8414–8424. [[CrossRef](#)] [[PubMed](#)]